Bulletin of the Seismological Society of America

THE SEISMOLOGICAL SOCIETY OF AMERICA
400 Evelyn Ave., Suite 201
Albany, CA 94706-1375
(510) 525-5474; FAX (510) 525-7204
www.seismosoc.org

Bulletin of the Seismological Society of America, Vol. 79, No. 3, pp. 731–755, June 1989

CONTEMPORARY TECTONICS OF THE WASATCH FRONT REGION, UTAH, FROM EARTHQUAKE FOCAL MECHANISMS

BY INGI T. BJARNASON* AND JAMES C. PECHMANN

ABSTRACT

We have completed a comprehensive study of focal mechanisms of digitally recorded earthquakes ($M_L \leqq 4.4$) that occurred in the Wasatch front region in Utah during 1980 to 1986. Single-event solutions for 24 events were determined using recently revised crustal models and a computerized grid-search technique.

Overall, the mechanisms show predominantly normal faulting on N-S-striking nodal planes of moderate to steep dip (>30°). Tension-axis azimuths average 96° ± 12°. Thus, in general, the mechanisms indicate E-W to ESE-WNW crustal extension and vertical crustal shortening. Oblique slip, when observed, is characterized by left-lateral motion on planes striking N to NE or right-lateral motion on planes striking N to NW. Most of the mechanisms with significant amounts of oblique-slip motion occur in the southern part of the study area, where compression-axis orientations range from near vertical to near horizontal. Thus, the mechanisms suggest a possible change in stress regime from north to south along the Wasatch front. Despite geologic evidence for low-angle faults in the study area, shallowly dipping nodal planes are relatively uncommon.

INTRODUCTION

The Wasatch fault zone and the associated physiographic escarpment known as the Wasatch front are situated at the eastern boundary of the Basin and Range Province in Utah (Fig. 1). To the east lie the Middle Rocky Mountains in the north and the Colorado Plateau in the south. The Basin and Range Province is characterized by extensional tectonism associated with late Cenozoic normal faulting. The Colorado Plateau is a late Cenozoic epeirogenic uplift which was formerly thought to have a laterally compressional stress field (Thompson and Zoback, 1979; Zoback and Zoback, 1980). However, recent work on focal mechanisms of earthquakes in the Colorado Plateau indicates that the compressional stress field is confined to the northwestern part of the plateau, and that most of the plateau is undergoing NE-SW extension (Wong *et al.*, 1987; Wong and Humphrey, 1989).

The Wasatch front region is considered to be an area of relatively high seismic hazard based both on historical seismicity and the presence of late Quaternary normal faulting (Fig. 1) (Gori and Hays, 1987). The 370-km-long northerly striking Wasatch fault zone extends from approximately the Utah-Idaho border on the north to 39°15′N on the south. Other active normal faults in the region include the East Cache fault and other subparallel range-bounding faults that generally lie to the west of the Wasatch and Cache Valley fault zones, with some exceptions (Fig. 1). Small to moderate earthquakes ($M_L < 6.5$) in the Utah region generally cannot be correlated with mapped Cenozoic faults, but instead form a broad diffuse zone of activity that is part of the N-S trending Intermountain seismic belt (Smith and Sbar, 1974; Arabasz *et al.*, 1980, 1987; Arabasz and Smith, 1981).

Earthquake focal mechanisms have been previously determined for the Wasatch front region by a number of authors and are summarized by Smith and Lindh

* Present address: Lamont-Doherty Geological Observatory and Department of Geological Sciences of Columbia University, Palisades, New York 10964.

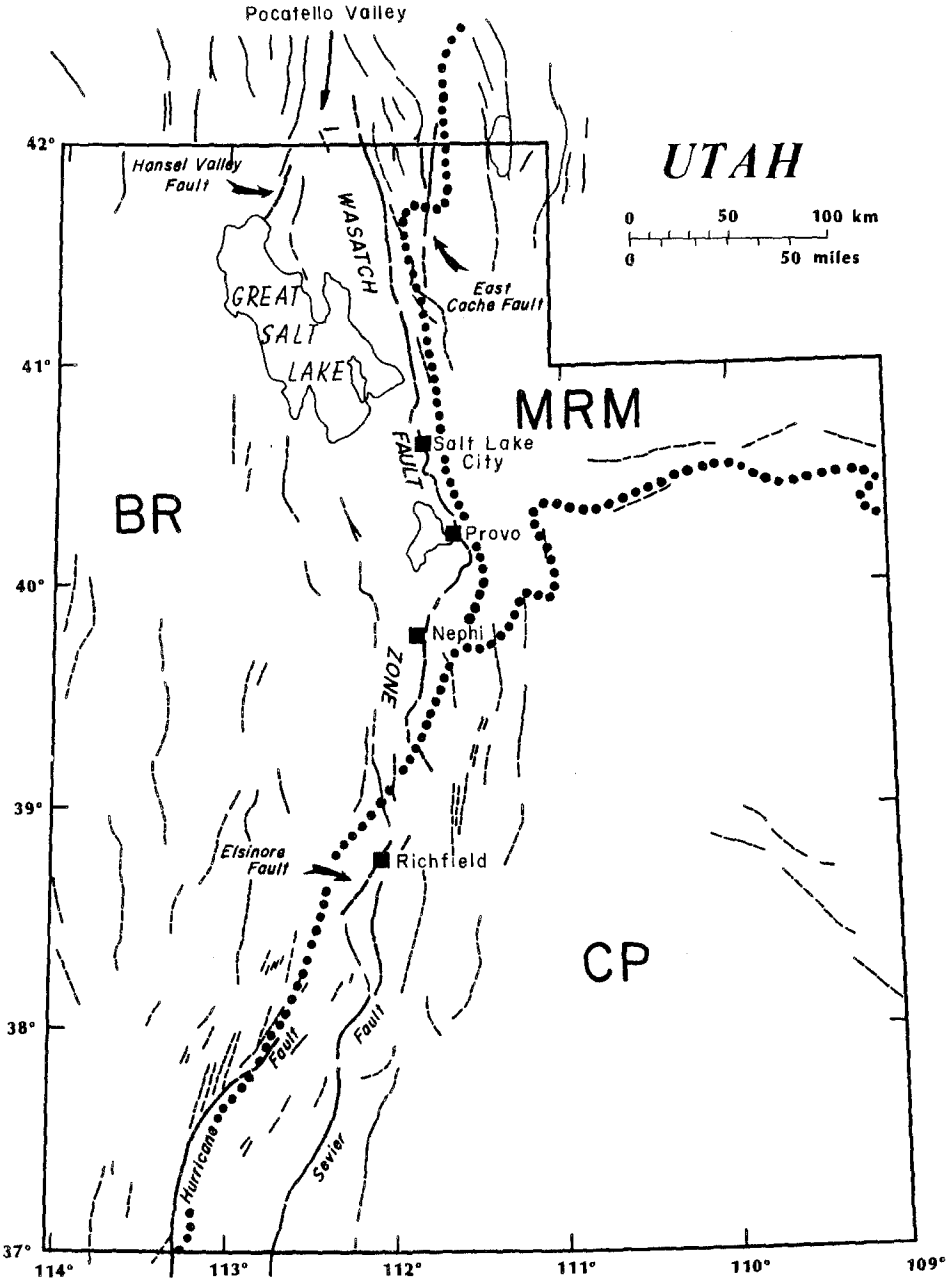

FIG. 1. Generalized map of late Cenozoic faulting in Utah, from Arabasz *et al.* (1979). The dotted lines indicate the boundaries between the Basin and Range (BR), Middle Rocky Mountains (MRM), and Colorado Plateau (CP) physiographic provinces (Fenneman, 1946).

(1978), Arabasz *et al.* (1980), and Zoback and Zoback (1980). Most solutions indicate normal faulting with an extension direction averaging approximately E-W. This differs from the generally WNW-ESE extension direction for the Basin and Range Province as a whole inferred from geological data, focal mechanisms, and *in situ* stress measurements (Zoback and Zoback, 1980; Zoback, 1983). Zoback (1983) used both slickenside data and focal mechanisms summarized by Arabasz *et al.* (1980) to

invert for orientations of the regional principal stress axes in the Wasatch front region. She concluded that the greatest principal stress was vertical and the least principal stress was oriented approximately E-W.

Farther south in Utah along the transition zone between the Basin and Range and the Colorado Plateau Provinces (37° to 40°N), focal mechanism data imply an extension direction that is closer to the general Basin and Range extension direction of WNW-ESE (Arabasz and Julander, 1986; Johnson and Sbar, 1987). In this region, the focal mechanisms suggest an eastward change from normal to strike-slip to mixed faulting, including reverse faulting (Arabasz and Julander, 1986). Thus, stress orientations in the southeastern part of the Wasatch front region may be influenced by the compressional tectonics of the northwestern part of the Colorado Plateau. Two reverse focal mechanisms have been reported 60-km SE of Salt Lake City, Utah, by Arabasz *et al.* (1980). However, according to W. J. Arabasz (personal comm., 1988), these reverse mechanisms may not be reliable because they are composite solutions based on data from the University of Utah fixed seismic network, and the hypocentral control for the earthquakes in the composites was less than ideal.

Improved data on earthquakes in Utah have become available due to expansion of the University of Utah seismic network in the late 1970's, and the initiation of digital recording of this network in January 1981. With the existing station density, it is possible to determine single-event focal mechanisms for some earthquakes as small as M_L 2.5 and most earthquakes of M_L 3.0 or greater in the Wasatch front region. This paper presents a systematic and comprehensive study of focal mechanisms for earthquakes in the Wasatch front region of $M_L \geqq 3.0$ that occurred during the time period 1 January 1981 to 30 June 1986. We chose to focus on earthquakes during this time period because of the high-quality digital data available for them. The boundaries of our study area (Fig. 2) are similar to those of the Wasatch front study areas of Arabasz *et al.* (1980) and Zoback (1983) but do not coincide exactly. We use these new focal mechanisms to investigate the style of faulting, subsurface faulting geometry, and regional stress field along the Wasatch front.

Focal Mechanisms Determinations

Data

The data for this study consists of *P*-wave arrival times and first-motion directions. These were obtained primarily from digital seismograms recorded by the University of Utah seismic network, which we displayed on a computer graphics terminal for analysis. Picks for the 24 May 1980 Goshen Valley earthquake (GOS, Table 1) were obtained from develocorder film records. For three earthquakes in central Utah, we augmented the University of Utah network data with additional film record readings from a seismic network in southestern Utah operated by Woodward-Clyde consultants. For event SC5 (Table 1), we used several readings from portable, smoked paper recorders that were installed by Brown *et al.* (1986) to record aftershocks of a M_L 4.4 earthquake on 24 March 1986, near Scipio, Utah (SC2, Table 1). Station polarities for the University of Utah stations were carefully verified, either by mechanically displacing the seismometer in the field or by examining first motions recorded from teleseisms and large explosions (Bjarnason, 1987).

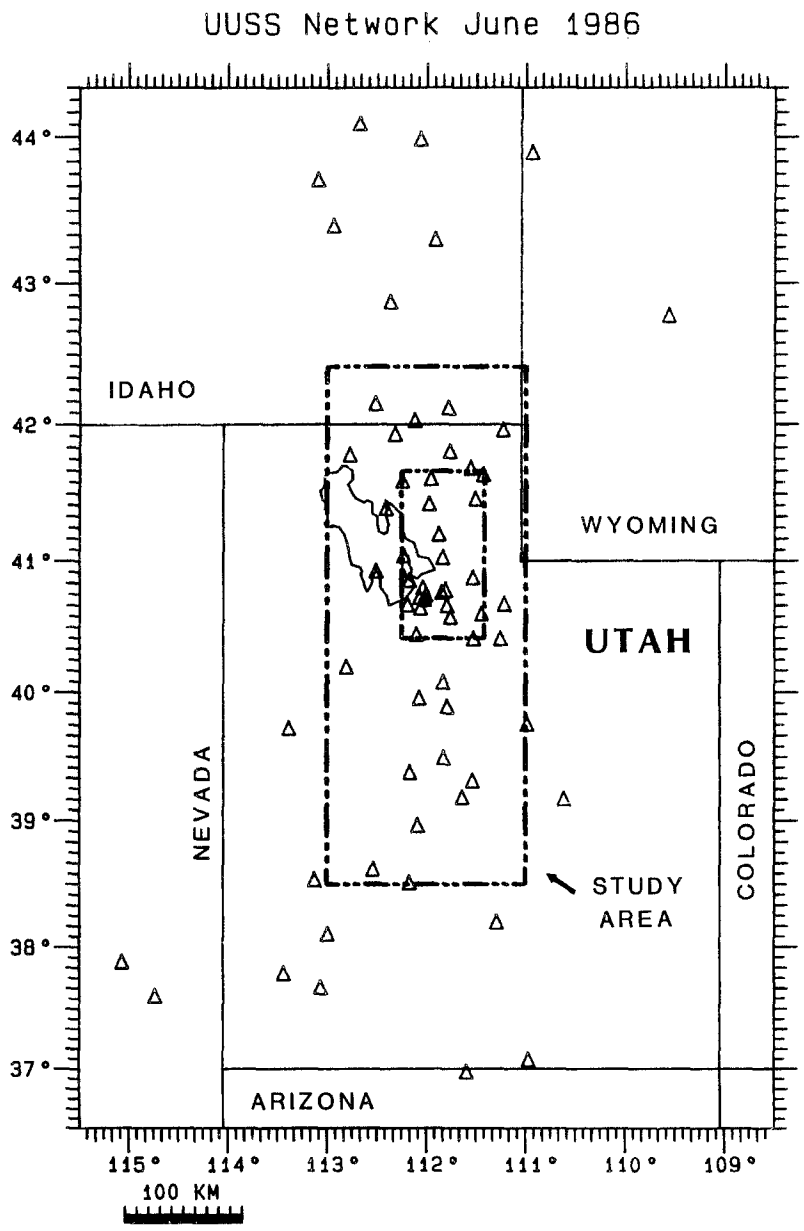

FIG. 2. The Univeristy of Utah Seismograph Stations network. Triangles indicate locations of the network stations as of June 1986. The larger dashed-dotted box outlines the study area. The smaller box denotes the part of the study area having the greatest station density, which allowed focal mechanisms for smaller earthquakes in this region to be determined.

Calculation of Locations and Takeoff Angles

One of the major sources of uncertainty in the determination of focal mechanisms of local earthquakes lies in the calculation of the takeoff angles for the first-arriving P waves. These angles depend upon both the crustal velocity structure and the location of the earthquake, especially its focal depth. Calculation of takeoff angles for Wasatch front earthquakes requires particular care because the focal depths are not, in general, well constrained and because the velocity structure is known to vary

TABLE 1

HYPOCENTRAL AND FOCAL MECHANISM PARAMETERS FOR WASATCH FRONT EARTHQUAKES, UTAH

Code	Date m/d/y	Time UTC	Location		Depth (km)	Magnitude (M_L)	Plane 1			Plane 2			Mechanism Quality
			Latitude (N)	Longitude (W)			Strike	Dip	Rake	Strike	Dip	Rake	
HV1	04/11/81	519	41°51.8′	112°41.3′	7.5	3.0	164	13	−47	301	80	−99	C
HV2	04/11/81	808	41°51.8′	112°40.8′	7.0*	3.1	14	79	−84	165	12	−119	B
HV3	05/12/84	1520	41°59.5′	112°32.7′	7.1	3.0	18	59	−62	153	41	−128	A
HV4	08/06/84	2230	41°52.5′	112°22.7′	5.4	3.0	212	46	−44	335	60	−127	B
HV5	02/21/86	2320	41°44.2′	112°48.9′	7.0*	3.6	32	49	−50	160	54	−126	B
BEL	01/28/82	800	42°23.7′	111°30.7′	3.0	3.2	156	46	−100	350	45	−80	A
LOG	01/13/86	1232	41°42.8′	111°39.7′	6.7	3.2	359	50	−108	205	43	−70	B
SWW	03/31/81	2040	41°41.6′	111°00.8′	1.0*	3.1	65	71	157	163	68	20	B
OG1	03/06/83	1053	41°8.7′	111°40.1′	11.6	2.8	353	47	−110	201	47	−70	B
OG2	06/05/86	741	41°16.0′	111°40.2′	11.4	2.8	224	86	−0	314	90	−176	C
OG3	06/05/86	805	41°16.3′	111°40.2′	12.1	3.6	356	61	−123	230	43	−46	A
BOU	08/29/82	1207	40°52.8′	111°39.9′	9.0*	2.7	353	28	−99	183	62	−85	B
SL1	10/08/83	1157	40°44.9′	111°59.5′	7.5*	4.3	174	33	−92	356	57	−89	A
SL2	06/10/84	1410	40°45.2′	112°03.9′	4.6	2.7 C	26	56	−41	142	57	−138	C
							201	44	−52	334	57	−121	
ORE	02/20/81	913	40°19.3′	111°44.1′	5.4	3.9	93	27	180	3	90	−63	A
GOS	05/24/80	1003	39°56.7′	111°58.3′	8.4	4.4	342	59	−139	227	56	−39	A
MIL	01/29/82	1209	39°29.5′	112°10.5′	12.0*	2.7	30	52	−49	155	54	−130	C
SC1	03/24/86	2233	39°12.7′	111°59.1′	6.3*	3.3	66	84	−36	160	54	−173	C
SC2	03/24/86	2240	39°13.4′	111°59.1′	6.3*	4.4	56	79	−45	157	46	−165	B
SC3	03/25/86	249	39°12.7′	111°59.3′	6.3*	2.8	356	61	−116	222	38	−52	C
							34	45	−65	181	50	−113	
SC4	03/25/86	253	39°13.1′	111°59.4′	6.3*	3.9	356	61	−116	222	38	−52	B
SC5	03/31/86	1753	39°13.8′	111°58.2′	5.6	1.0 C	41	58	−56	170	45	−131	C
WAP	01/08/84	159	39°2.1′	111°28.7′	0.6	2.7	122	78	167	215	78	12	A
COF	12/09/83	858	38°34.5′	112°33.3′	3.1	3.6	334	60	−144	224	59	−36	A

* Fixed depth

C = Coda magnitude

Rake angles and strikes are defined according to the convention of Aki and Richards (1980).

laterally. The ideal approach to the latter problem would be to use a three-dimensional velocity model for the calculations. Unfortunately, a three-dimensional velocity model adequate for this purpose does not exist for Utah. The problem of lateral velocity variations is minimized to some extent by the geometry of the University of Utah network, which is elongated in a N-S direction parallel to the physiographic province boundaries and to the strike of a regional structure (Figs. 1 and 2). Therefore, in this study we approximate the lateral variations in the velocity structure by using three one-dimensional velocity models, as described below.

Earthquake locations and takeoff angles for first-arrival ray paths were calculated with the location program HYPOINVERSE (Klein, 1978). For most of the stations in the network, we used a horizontally layered velocity model for the Wasatch front modified from model B of Keller *et al.* (1975) (Table 2). Keller *et al.* derived their model using data from an unreversed seismic refraction profile beginning at an open-pit mine near Salt Lake City and extending 245-km southward along the Basin and Range/Colorado Plateau transition zone. Our modifications to their model consisted of (1) the addition of a 7.9 km/sec halfspace beginning at a depth of 42 km, and (2) an increase in the depth of the top of their 7.5 km/sec layer from 25.4 km to 28 km. These modifications are based on interpretations of travel-time data from local and near-regional earthquakes and blasts recorded on the University

TABLE 2
VELOCITY MODELS

Region	*P*-Wave Velocity (km/sec)	Depth to Top of Layer (km)*
Wasatch front	3.4	0.0
	5.9	1.5
	6.4	17.1
	7.5	28.0
	7.9	42.0
Colorado Plateau	3.4	0.0
	5.9	1.5
	6.2	17.1
	6.8	27.5
	7.9	42.0
Southeast Idaho	3.4	0.0
	5.9	1.5
	6.8	17.1
	7.9	42.0

* Datum is 1500 m above sea level

of Utah seismic network (Pechmann *et al.*, 1984; Loeb, 1986; Loeb and Pechmann, 1986). Both the 7.5 km/sec and 7.9 km/sec refractors dip to the east beneath the Wasatch front. The depths of these refractors in our horizontally layered model were chosen to be their average depths beneath the central part of the University of Utah network. The increased depth of the 7.5 km/sec layer was proportionately distributed to all the layers above it, for consistency with the velocity models of Loeb (1986) and Loeb and Pechmann (1986).

Although the bulk of our first-motion readings are from stations in the Wasatch front region, it was sometimes possible to get reliable data from stations in SE Idaho or in the Colorado Plateau of SE Utah. The velocity structures in these two regions differ significantly from the velocity structure of the Wasatch front because of the absence of the 7.5 km/sec refractor (Loeb, 1986; Loeb and Pechmann, 1986). To calculate takeoff angles for stations in SE Idaho and in the Colorado Plateau, we used the one-dimensional velocity models for these regions given in Table 2. These models were assigned the same velocities in the upper crust (<17.1 km) as the Wasatch front model. Since all the earthquakes of this study are located in the Wasatch front region, this ensures that the correct near-source velocity is used for the ray-path calculations. Most of the first-arriving phases to the Colorado Plateau and SE Idaho stations of this study are refracted waves. It is reasonable to assume that as they travel deeper into the lower crust and into the upper mantle, they will be entering into the velocity structure of the Colorado Plateau or SE Idaho. Therefore, below 17.1 km the models have velocities appropriate for the Colorado Plateau or SE Idaho regions, as determined by seismic refraction work (Roller, 1965; Sparlin *et al.*, 1982).

Accuracy of Takeoff Angles

In order to calculate the source takeoff angle for a ray that travels through a horizontally layered medium, it is necessary to know only the near-source velocity and the slope of the travel-time curve at the recording station. This follows from

Snell's law (1) and Benndorf's relation (2):

$$p = \frac{\sin i(z)}{v(z)} \tag{1}$$

$$p = \frac{dt}{d\Delta}, \tag{2}$$

where p is the ray parameter, i is the takeoff angle at the hypocenter between the ray and the vertical z axis, v is the velocity near the source, t is the travel time, and Δ is the horizontal distance between the epicenter and the recording station. Therefore, if there is good agreement between the observed travel times and those computed from a particular velocity model, takeoff angles calculated using this model are unlikely to be greatly in error provided that the estimate of the near-source velocity is accurate.

As a check on the takeoff angles, we constructed a reduced travel-time plot for every earthquake used in this study. Figure 3 shows two examples. Note that the travel times calculated from the Wasatch front velocity model in Table 2 and shown

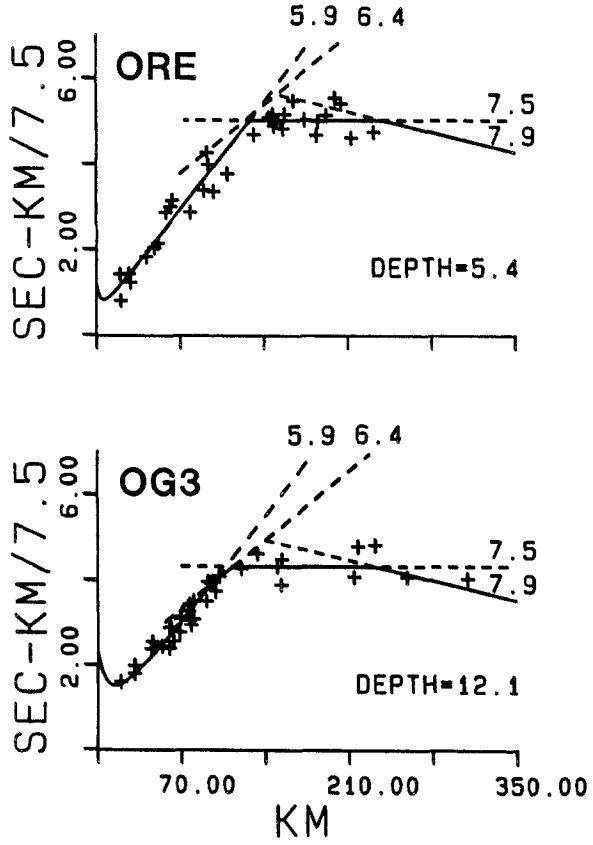

FIG. 3. Reduced travel-time plots of first-arriving P waves (plotted as +'s) for two Wasatch front earthquakes. The reducing velocity is 7.5 km/sec. The solid lines labeled with velocity in km/sec indicate theoretical travel times calculated from the Wasatch front velocity model (Table 2). The location program has set the focal depths primarily to match the arrival times of the 7.5 km/sec arrivals between about 120 and 250 km epicentral distance. The top event (ORE) has an apparent depth of 5.4 km and the bottom event (OG3) has an apparent depth of 12.1 km.

as solid lines fit the data quite well. Most of the data fall onto two branches of the travel-time curves: a *Pg* branch consisting of direct arrivals with a velocity near 5.9 km/sec, and a P^* branch between about 120 and 250 km epicentral distance consisting of refracted waves with a velocity near 7.5 km/sec. For both of the earthquakes in Figure 3, the closest stations are at epicentral distances of more than 19 km and therefore provide very little constraint on focal depth. The location program has set the focal depths to match the arrival times of the refracted waves, which were used in the locations but down weighted using a distance weighting factor that was equal to one for stations closer than 120 km, zero for stations beyond 250 km, and followed a cosine taper in between (see Klein, 1978). For earthquakes for which we observed a systematic difference between the calculated and observed travel times of the refracted waves, we fixed the focal depth in order to obtain an agreement between them and then recalculated the takeoff angles.

Adjustment of the focal depths to match the 7.5 km/sec refracted arrivals is justified because very few earthquakes used in this study have well-constrained focal depths. The generally poor depth control is a consequence of the relatively large average station spacing within the network (Fig. 2), which typically results in a lack of stations within one focal depth of the epicenter. Matching the observed and calculated travel times for the refracted waves serves to assign each reading to the proper branch of the travel-time curve and thus produces realistic takeoff angle assignments. Some uncertainty still remains regarding the takeoff angles for first arrivals recorded near crossover distances, such as the Pg-P^* crossover. Misidentification of these arrivals can lead to large errors in takeoff angles of up to 38°. If changing the takeoff angles for stations near crossover distances had a radical effect on a particular focal mechanism, it was discarded as unconstrained.

The approximation of the eastward-dipping 7.5 km/sec and 7.9 km/sec refractors by horizontal layers in the Wasatch front velocity model should not cause significant errors in the takeoff angle calculations, provided that the refracted waves are properly identified. The University of Utah network is elongated in a N-S direction parallel to the strike of these refractors (Fig. 2). Therefore, the apparent dips of these refractors in the direction of propagation of the refracted waves should generally be smaller than the true dips of the refractors, which are 6° or less (Loeb, 1986).

Estimates of near-source velocities for Wasatch front earthquakes are fortunately not very sensitive to focal depth. The *P*-wave velocity in our Wasatch front model is 5.9 km/sec over the depth range of 1.5 to 17.1 km (Table 2). As discussed below, this is the depth range within which the great majority of the earthquakes occur. Interpretations of refraction data from four profiles available in the study area show velocities of 5.7 to 6.1 km/sec beginning at 1 to 2 km depth and extending down to 12 to 15 km depth, except within possible crustal low-velocity zones (Braile *et al.*, 1974; Keller *et al.*, 1975; Martin, 1978; Muller and Mueller, 1979). Within the crustal low-velocity zones that are included in some of the proposed refraction models the velocities decrease to 5.2 to 5.8 km/sec. Material in the upper crust with a velocity of 5.7 to 6.1 km/sec typically consists of 'crystalline basement' (e.g., Mueller, 1977; Meissner, 1986). However, well-logging data show that some Paleozoic sedimentary rocks in Utah have velocities comparable to those of the underlying crystalline basement (Braile *et al.*, 1974; Julander, 1983; W. J. Arabasz, written comm., 1986). Considering both lateral and vertical velocity variations that are likely to occur within the seismogenic zone in the study area, we believe that the near-source velocity is probably 5.9 ± 0.2 km/sec for most of our earthquakes. The corresponding

uncertainty in takeoff angle is 5° or less for refracted waves but up to 15° for *Pg*. More severe errors in takeoff angle could occur for sources located within a strong low velocity zone.

Available data suggest that it is reasonable to assume that most small ($M_L < 5.0$) earthquakes in the Wasatch front region have focal depths in the upper crust below the low-velocity surface layer. This has been observed in microearthquake studies along the Wasatch front that employed dense, portable networks to obtain good focal depth (Arabasz *et al.*, 1981; Arabasz and Julander, 1986). Further supporting evidence comes from an examination of focal depths of earthquakes of $M \geqq 2.0$ from the years 1962 to 1986 that occurred within the study area and have at least one station within 5 km from the epicenter (Fig. 4). This sorting method does not discriminate against shallow earthquakes and should select, on the average, earthquakes with better constrained focal deths. Of the earthquakes examined, 92 per cent had focal depths lying within the depth range 1.5 to 17.5 km and the remainder had focal depths lying within 0- to 1.5-km depth. There is a peak in the depth distribution between 4.5 and 6.0 km and the mean depth is 5.5 km. Note that this peak is not an artifact of the starting depth for the catalog locations, which is 7 km. Thus, from Figure 4 it appears that very few Wasatch front earthquakes of $M \geqq 2$ occur outside the depth range of the 5.9 km/sec layer in our velocity models.

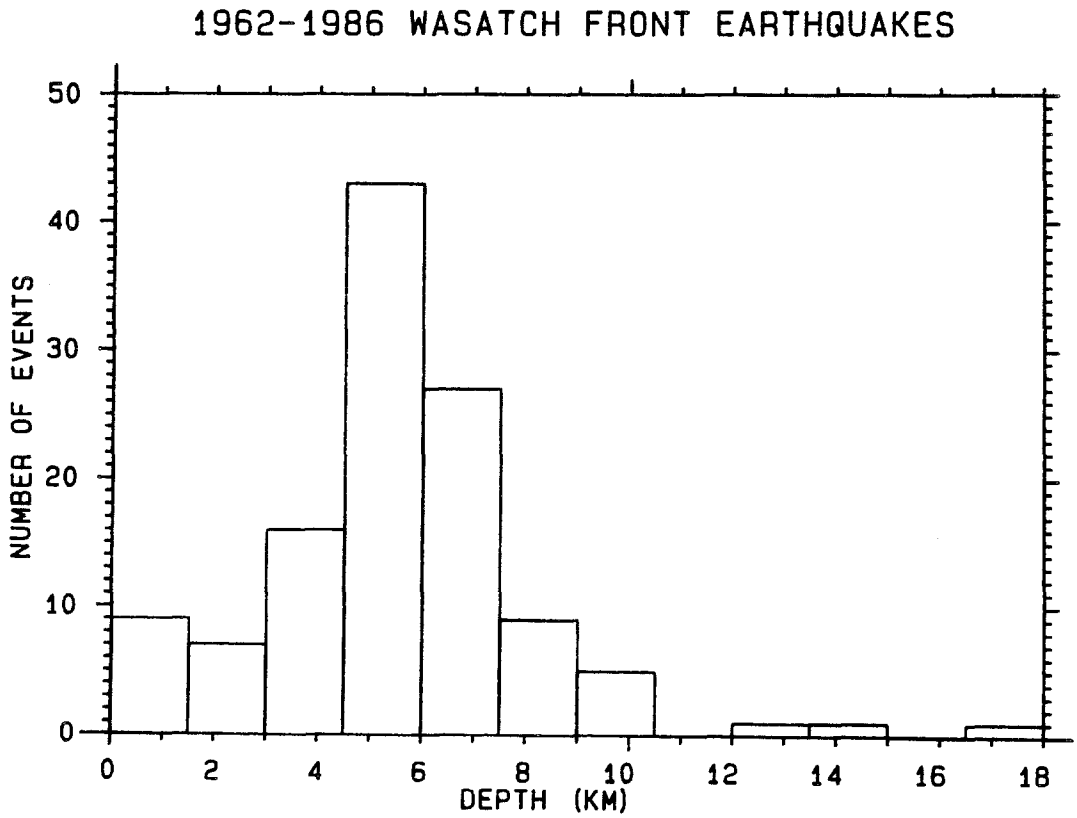

FIG. 4. Histogram of focal depths for Wasatch front region earthquakes of magnitude greater than or equal to 2.0 from July 1962 to June 1986. The plot only includes earthquakes for which at least one station within 5 km of the epicenter was used in the location.

Determination of Nodal Planes

The nodal planes of the focal mechanisms were determined with the aid of the computer program FOCPLT developed by Whitcomb and Garmany (Whitcomb, 1973). This program provides fast, objective nodal plane determinations along with estimates of uncertainty in the orientations of the slip vectors and the compression (P) and tension (T) axes. This is done by searching through a large number of mechanisms with the poles of successive trial nodal planes spaced approximately 5° apart on the focal sphere and determining the number of first-motion readings in error for each. For each trial mechanism, the program calculates a misfit score that depends on the number of first-motion readings in error, the quality of these readings, and their distance from the nodal planes. We gave full weight to first-motion readings for which the signal-to-noise ratio was 3 or greater and half weight to readings for which the signal-to-noise ratio was between 2 and 3. We did not use first motions that were less than a factor of 2 above the noise. Stations near a nodal plane are down weighted using a linear weighting function having a value of 0 on the nodal plane and 1 at a distance of 3° from the nodal plane. After calculating the weighted scores for each focal mechanism, the program chooses the mechanism with the lowest score. When two or more mechanisms fit the first-motion data equally well, the program selects a mechanism that represents an average of the different possible solutions.

RESULTS

We attempted to determine a focal mechanism for every earthquake of $M_L \geqq 3.0$ that occurred in the Wasatch front study area (Fig. 5) from 1 January 1981 to 30 June 1986, and for which digital data were available. To augment the areal coverage, we also determined focal mechanisms for one M_L 4.4 event in 1980, and for eight smaller earthquakes of $M_L < 3.0$. Seismograms of earthquakes in Utah with magnitudes less than 3.0 generally do not show many clear first motions at distances beyond about 120 km, where the first arrivals are refracted waves. This makes it difficult to construct well-constrained focal mechanisms for $M_L < 3.0$ events unless they are favorably located within the network (for example, within the smaller box in Fig. 2) or else supplementary data from portable seismographs are available.

From the 35 earthquakes that we analyzed, we were able to obtain 24 focal mechanism solutions of reasonable good quality. These 24 focal mechanisms are presented in Table 1 and Figures 6 and 7. The hachured regions or squares around the slip vectors on the first-motion plots in Figure 6 show the locus of slip vector positions that correspond to the 'good' solutions. The regions between the good solutions and the dashed lines correspond to 'fair' solutions. A good solution is defined to be a mechanism with the minimum number of first-motion readings in error, that is, a best-fit solution. A fair solution has up to one full-weight or two half-weight first-motion readings in error beyond the minimum. Note that good and fair are relative descriptions of the quality of the mechanism for an individual earthquake. A fair focal mechanism of one earthquake can have fewer stations in error than a good mechanism of another earthquake.

We consider only eight of the focal mechanisms in Figure 6 to be well constrained. For these mechanisms (quality A, Table 1), the slip vectors for the good solutions occupy small areas of the focal sphere and the fair solutions are very similar to the good solutions. The remaining 16 mechanisms are well constrained if only the good solutions are considered, but they can have significantly different nodal plane

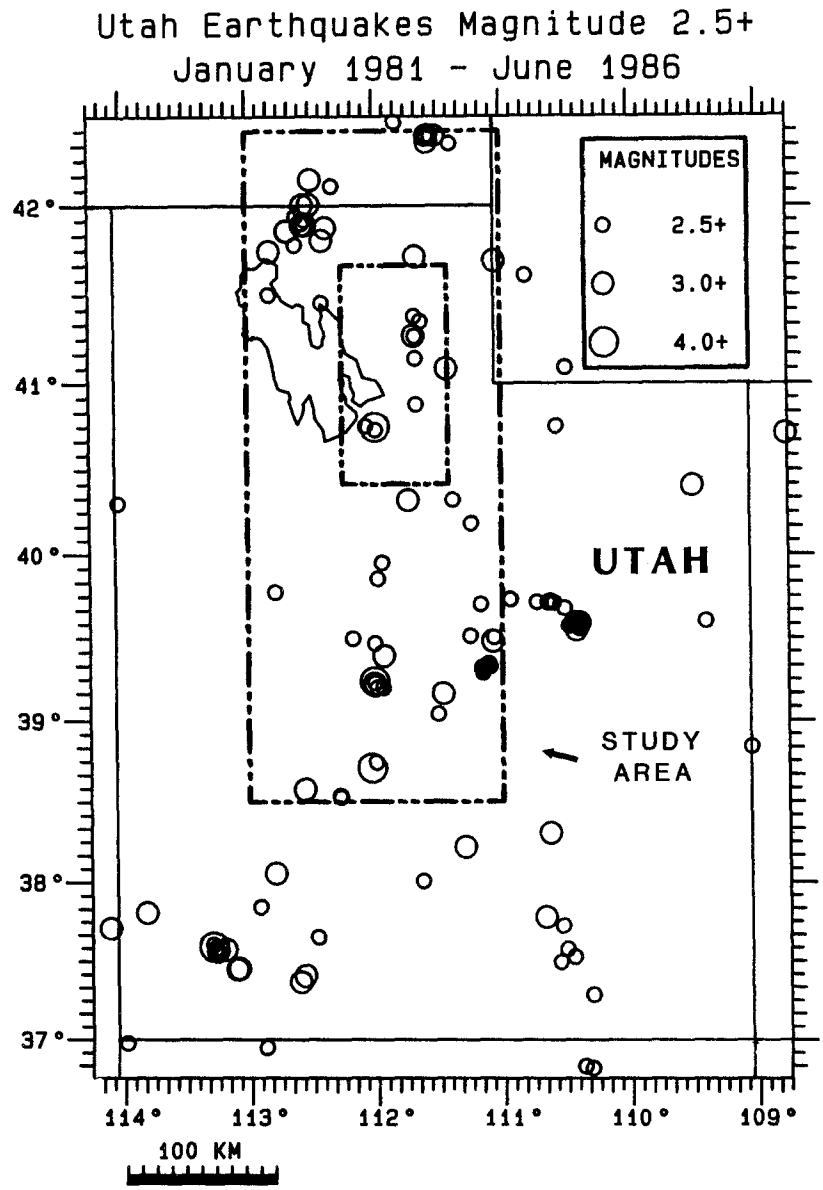

FIG. 5. Seismicity map for the Utah region. The circles indicate epicenters of events with $M \geqq 2.5$ that occurred from January 1981 through June 1986.

orientations when the fair solutions are taken into account. We assigned these mechanisms quality ratings of either B or C, depending on the amount of variability among the good solutions (Table 1, Fig. 6). The mechanism for SWW would appear from the contours in Figure 6 to be an A quality solution, but we gave it a B rating because the nodal plane orientations are somewhat sensitive to focal depth.

Most of the focal mechanisms show normal faulting with a small amount of oblique slip (Figs. 6, 7; Table 1). Two strike-slip solutions, OG2 and WAP, and one oblique-reverse solution, SWW, were also observed. In general, the mechanisms in the southern part of the study area appear to have larger components of strike-slip motion than the mechanisms in the northern part. In both parts of the study area,

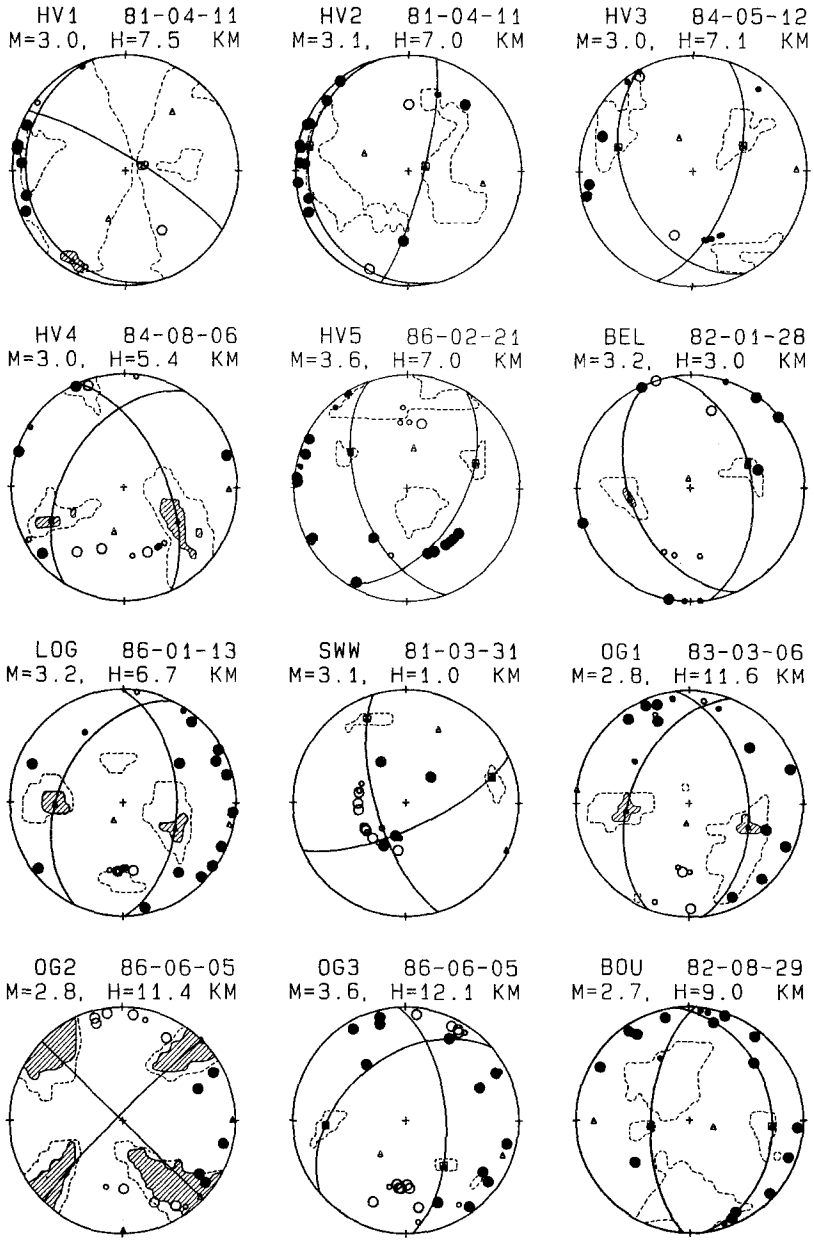

FIG. 6. *P*-wave first motions plotted on equal-area lower hemisphere diagrams for 24 earthquakes within the study area. Solid circles represent compressions and open circles dilatations. Larger circles indicate full-weight readings and smaller circles half-weight readings. Triangles represent *P* axes, *T* axes, and slip vectors. The hachured areas or squares around the slip vectors represent the range of positions for slip vectors corresponding to 'good' solutions, i.e., those having the minimum number of readings in error. Areas between the dashed lines and hachured areas denote positions of slip vectors for 'fair' focal mechanisms, which have up to one full-weight reading or two half-weight readings in error beyond the minimum. For each earthquake its code, date, magnitude (M), and depth (H) are given.

when oblique slip is observed, N- to NW-striking nodal planes have a right-lateral strike-slip component, while N- to NE-striking nodal planes have a left-lateral strike-slip component. The oblique-reverse focal mechanism for SWW is an exception to this general trend.

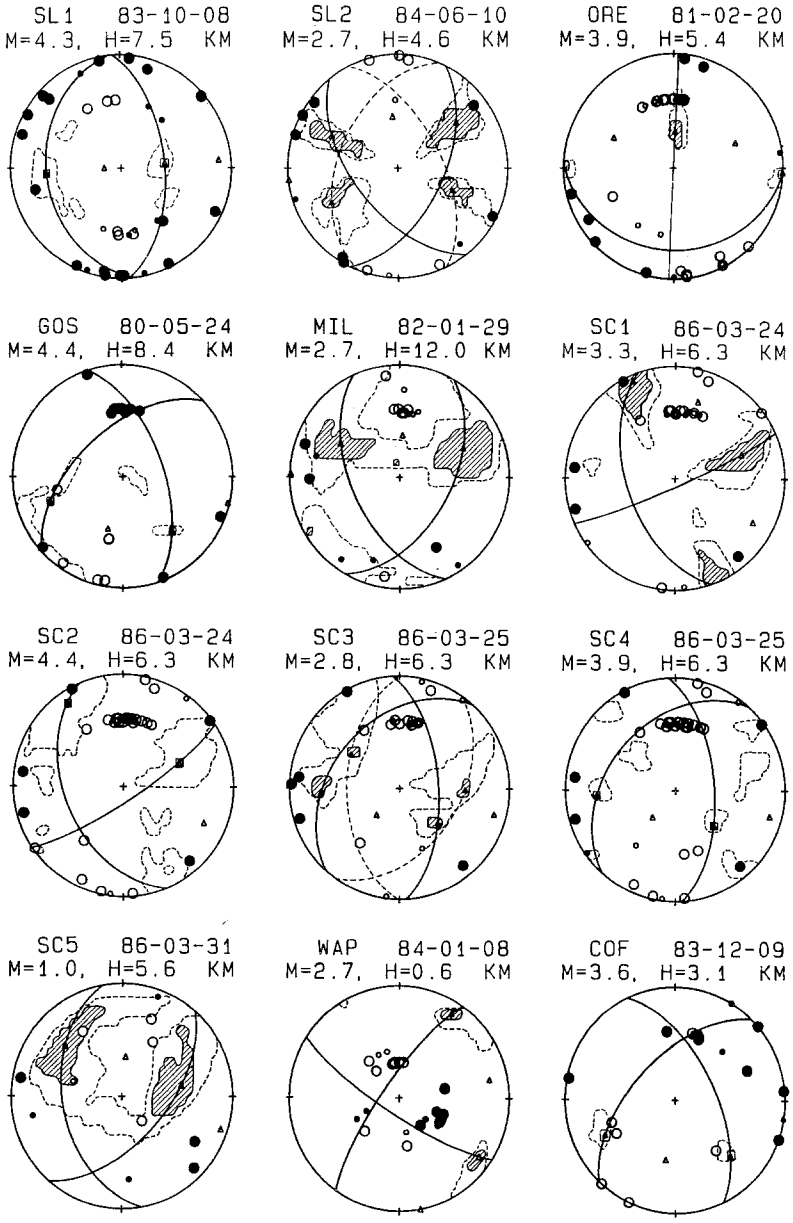

Despite geological and geophysical evidence for low-angle faults in the study area (e.g., Smith and Bruhn, 1984), only 4 of the 24 events had one possible nodal plane with a shallow dip (<30°) (Table 1). It is noteworthy that the mechanisms for events HV1 and HV2, which occurred on the same day within 1 km of each other, have a common nodal plane which is low angle. Unfortunately, the HV1 mechanism is one of the least-constrained focal mechanisms of the 24, when the 'fair' solutions are taken into account.

The foreshock-main shock pair OG2 and OG3 shows an interesting sequence of strike-slip faulting followed by oblique normal faulting. The NW-dipping nodal plane of the main shock can also be made to fit the first-motion data of the

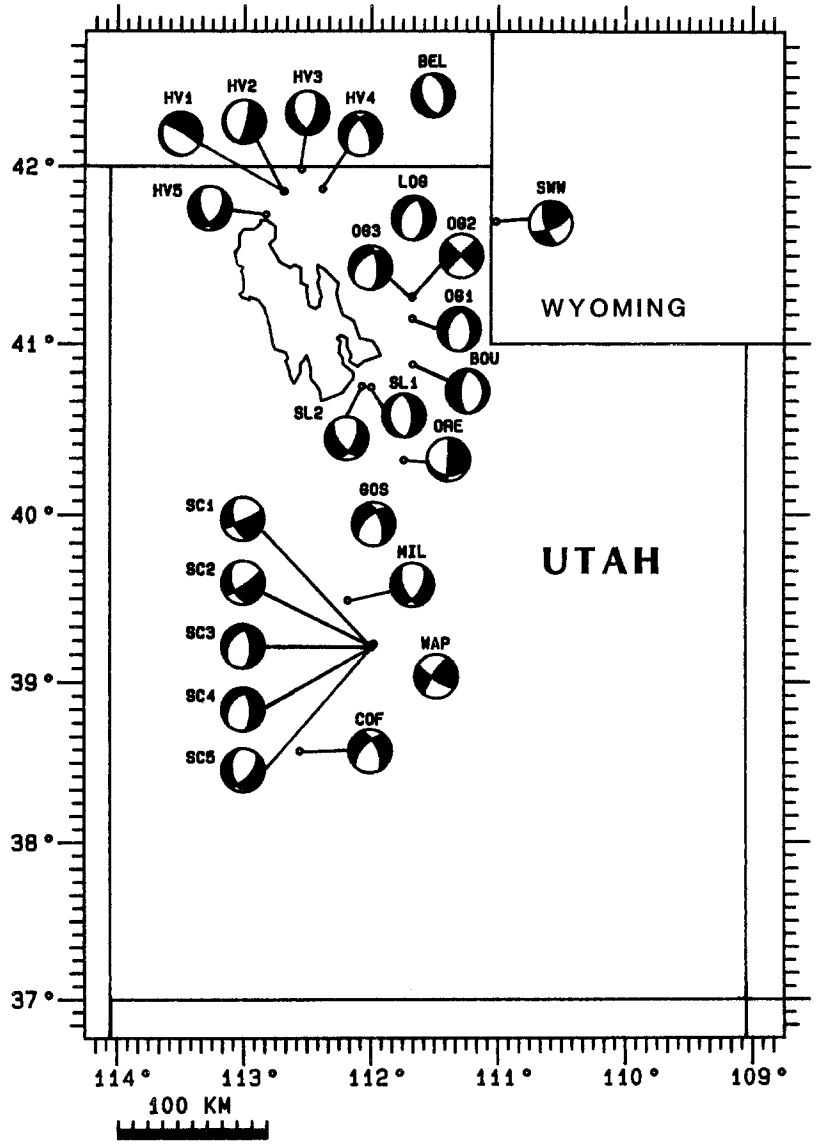

FIG. 7. Summary map of focal mechanisms from Figure 6. Compressional quadrants are black and dilatational quadrants are white. Small circles are epicenters for the earthquakes. Focal mechanisms not connected to a circle are centered on the epicenter.

foreshock exactly, but the E-dipping nodal plane of the main shock cannot be made to fit the first motions of the foreshock. This could be an indication that the NW-dipping nodal plane of the main shock is the fault plane for both events. As the location of the foreshock is almost indistinguishable from the main shock, it cannot be argued that the difference in the focal mechanisms is a result of an interchange of principal stress directions due to an increase in the vertical stress as a function of depth (e.g., Vetter and Ryall, 1983). A similar contrast in focal mechanisms for earthquakes in the same sequence has been observed before along the Wasatch front near Richfield, Utah (Fig. 1). Here, an M_L 4.0 main shock with a normal or oblique-normal focal mechanism was followed by strike-slip aftershocks (Arabasz and Julander, 1986).

The focal depths of the Scipio earthquake sequence, events SC1 to SC4, were fixed at 6.3 ± 2 km (Table 1). This depth was based on reduced travel-time curves for these events and on the focal depth distribution of aftershocks located with a portable network installed after the M_L 4.4 main shock (Brown *et al.*, 1986). Even though the depth to the 'crystalline basement' at this location is approximately 10 km, the Wasatch front velocity model (Table 2) is still applicable, because nearby well-logs show sedimentary rocks below 3 km to have velocity of 5.8 km/sec (W. J. Arabasz, written commun., 1986).

Two earthquakes of this study, WAP and SWW, were located within the surface layer of the Wasatch front velocity model (Tables 1 and 2). The reduced travel-time curves for these earthquakes suggest that they are very shallow. The WAP event is located near an active coal mining area of east-central Utah. Microearthquake studies in this area suggest that part of the seismicity is mining-induced and that most events lie between 0- and 4-km below the surface (McKee and Arabasz, 1982; Williams and Arabasz, 1985, 1989; Arabasz and Julander, 1986). This is an area of high elevation where the surface layer is generally thicker and of higher velocity than in most other parts of the study area (McKee and Arabasz, 1982; Julander, 1983; Arabasz and Julander, 1986). Tests show that the nodal planes of the WAP event are not sensitive to the velocity or thickness of the surface layer nor to focal depth. Therefore the free depth WAP mechanism, for which the standard Wasatch front velocity model was used (Table 2), is a reliable solution. The SWW earthquake is located near the Utah-Wyoming border in the Middle Rocky Mountains province. The one-dimensional Wasatch front velocity model may not be reliable for an earthquake this far east of the center of the recording network. The expected delay in travel times of refracted waves caused by the eastward dip of the 7.5 km/sec and 7.9 km/sec refractors could make the focal depth of this event appear to be more shallow than it is. Nevertheless, the mechanism with a focal depth in the surficial layer provided the most consistent fit to the first-motion data, and was therefore selected as the most plausible mechanism for this earthquake. The SWW mechanism is somewhat sensitive to focal depth, but tests indicate a reverse component of slip regardless of the focal depth.

As only one third of our focal mechanism can be considered to be well constrained and the remainder are only moderately well constrained, it is advantageous to look at them as a group using an averaging technique that takes into account the degree of constraint of the individual mechanisms. This was done by combining the grids of scores for the individual focal mechanisms to make composite grid score plots for the slip vectors, compression (P) axes, and tension (T) axes. The SWW mechanism was not included in the composite plots, as it appears to be more closely related to the tectonics of the Middle Rocky Mountains than to the eastern Basin and Range. To create the composite plots, we calculated a weighted average grid score at each grid point, expressed as a percentage of the maximum possible score. The weighting scheme that was used assigns a weight of 3 to grid points of 'good' solutions, a weight of 2 to 'fair' solutions, a weight of 1 to solutions with 1 to 2 full weight or 2 to 4 half-weight first-motion readings in error beyond the minimum, and 0 weight to other solutions. Finally, the grid point scores were contoured using an contour interval of 10 per cent starting with the 30 per cent contour line (Fig. 8).

The weighting scheme used can introduce a bias into the composite plots because all of the mechanisms are given equal weight but the range of possible solutions for the less well-constrained mechanisms is larger. On the other hand, it is also

important to give the 'fair' solutions a significant weight in the averaging scheme because this helps to take into account errors in takeoff angles and possible observational errors in first-motion picks.

Figure 8 (top) shows the focal mechanism composite plots for the entire Wasatch front study area. The composite tension-axis contours suggest a very consistent extension direction that is approximately E-W to ESE-WNW and nearly horizontal. The composite compression-axis contours extend over a broader zone plunging between 30°N and 45°SSW. The average focal mechanism deduced from these plots (upper right, Fig. 8) is characterized by normal faulting on moderately dipping planes that strike approximately N-S.

As mentioned before, it appears that more mechanisms in the southern part of the study area have large components of oblique slip than do mechanisms in the northern part (Fig. 7). For this reason, the study area was split up into northern and southern regions and composite plots made for each of them in order to test quantitatively for systematic regional differences in focal mechanisms. The division was made at 40°N, which is approximately the northern limit of the Basin and Range/Colorado Plateau transition zone (Arabasz and Julander, 1986). It also

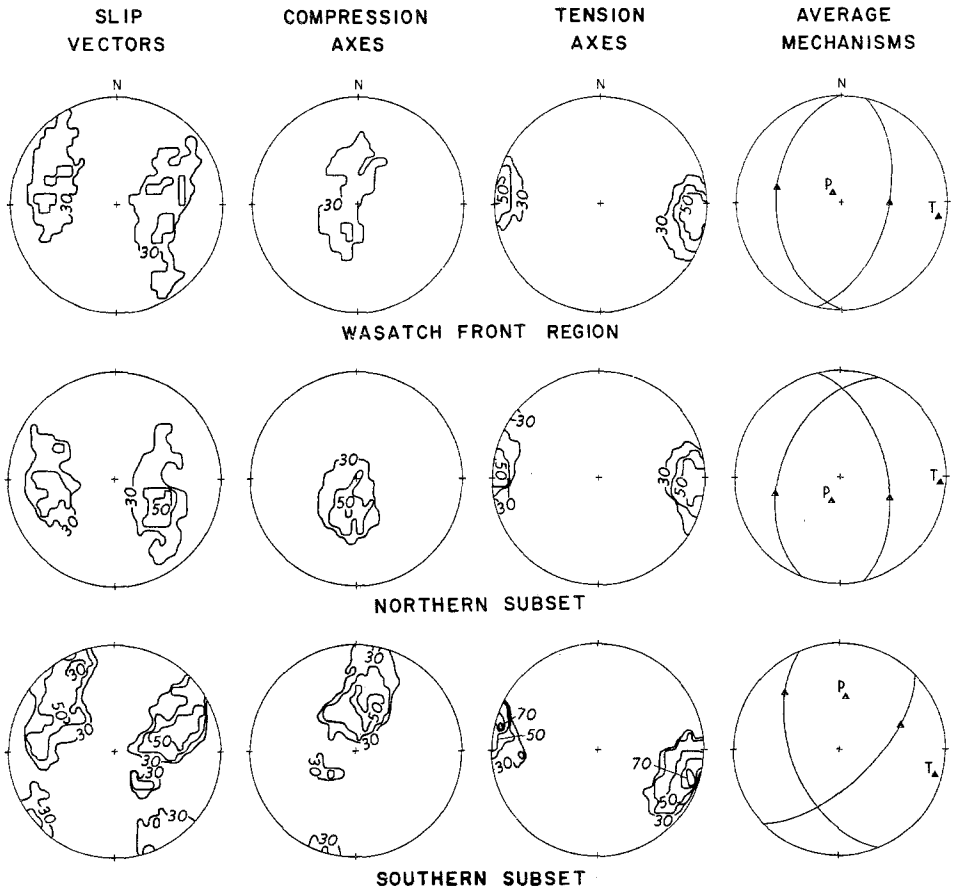

FIG. 8. Composite grid score plots. The top row shows plots of weighted average grid scores, expressed as a percentage of the maximum possible score, for 23 of the focal mechanisms (SWW was excluded). Contour interval is 10 per cent. See text for further explanation. The average mechanism for these 23 events as deduced from the composite plots is shown with triangles representing the P axis, T axis, and slip vectors. The center and bottom rows show analogous plots for subsets of the 23 focal mechanisms located north and south of 40°N, respectively.

coincides with the boundary between the Provo and Nephi segments of the Wasatch fault zone, as defined by Schwartz and Coppersmith (1984). The Wasatch fault zone turns at this boundary from a generally NNW strike north of it to a NNE strike south of it (Fig. 1).

Figure 8 demonstrates that, on the average, there is a significant difference in focal mechanism parameters between the northern and southern parts of the study area. In the northern region, the compression axes plunge on the average steeply towards the SSW, while in the southern region, the compression axes plunge from near vertical to near horizontal in a NNE direction. This regional difference in P-axis orientations explains the lack of a well-defined average P-axis orientation for the study area as a whole. The tension-axis contours define the average T-axis direction to be approximately E-W in the northern Wasatch front and ESE-WNW in the southern Wasatch front. This small difference in T-axis orientations may not be significant because of the large overlap between the contoured regions on the T-axis plots for these two areas (Fig. 8).

The average focal mechanism for the northern region is very well constrained by the maxima of the slip vector, compression-axis, and tension-axis plots, indicating very uniform focal mechanisms for earthquakes in this region. It suggests normal faulting with moderately dipping nodal planes striking approximately NNW to NNE. The slip-vector and compression-axis distributions for the southern mechanisms are more diffuse than those of the northern ones, indicating a greater variety of mechanisms in this region. This can also be seen in Figure 7, but not as clearly. The average mechanisms for the southern region suggests normal faulting with a large strike-slip component and has nodal planes striking approximately NNW and NE.

Discussion

Of the focal mechanism parameters presented in Figure 8, the tension axes have the most clearly defined preferred directions. For comparison with Figure 8, Figure 9 shows P and T axes for microearthquake ($M < 2.0$) focal mechanisms in Hansel and Pocatello Valleys determined by Jones *et al.* (1985) (see also Jones, 1987) together with those of Arabasz and Julander (1986) for earthquakes ($M \leqq 5.6$) in the Basin and Range/Colorado Plateau transition zone. The T axes from both studies cluster near the horizontal between ENE-WSW and SE-NW. Arabasz and Julander calculated a mean T-axis orientation of 102° ± 21° (one S.D. error bar) from the 30 T axes in their data set having a plunge less than 30°. The 16 T axes in the Jones *et al.* data set with a plunge less than 30° have a mean orientation of 104° ± 28°, which is nearly the same as the value calculated by Arabasz and Julander. The T axes from these two studies are consistent with our results (Fig. 8), but do not support the suggestion in Figure 8 of a change in extension direction between the northern and southern parts of the Wasatch front region.

Of the 24 focal mechanisms in our data set, all but three (HV1, HV2, and ORE) have T axes with a plunge of less than 30° (Fig. 6). Excluding these three mechanisms and the oblique-reverse mechanism SWW, the remaining 20 focal mechanisms have a mean T-axis orientation of 96° ± 12° (one S.D. error bar). The azimuth range 96° ± 12° corresponds almost exactly to the range bounded by the 50 per cent contours on the T-axis plot for the whole study area (Fig. 8, top). This range also encompasses the mean T-axis directions for the focal mechanisms of Jones *et al.* (1985) and Arabasz and Julander (1986). Thus, the T-axis diagrams in Figures 8 and 9 provide

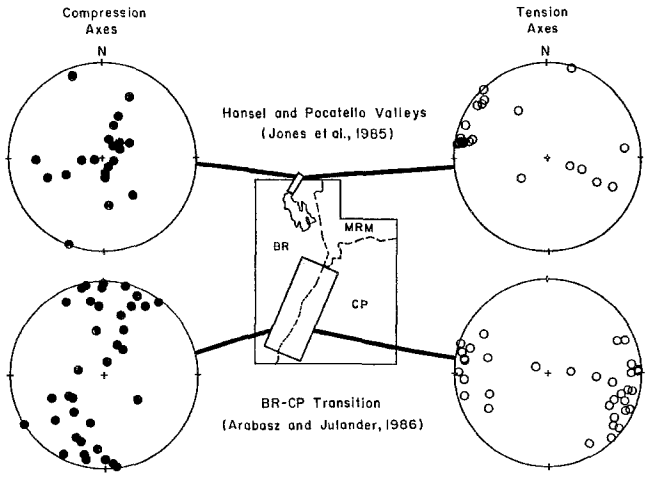

FIG. 9. Compression and tension axes for focal mechanisms of Utah earthquakes determined in studies using portable seismographs. These data are from studies by Jones *et al.* (1985) and Arabasz and Julander (1986). Their study areas are indicated with boxes. The compression and tension axes from Jones *et al.* (1985) are from A, B, and C quality focal mechanisms determined with the one-dimensional velocity model M8 (Jones, 1987). The dashed lines are the physiographic boundaries between the Basin and Range (BR), the Middle Rocky Mountains (MRM), and the Colorado Plateau (CP) provinces (Fenneman, 1946).

strong evidence for contemporary EW to ESE-WNW extension along the Wasatch front in Utah.

Figure 8 shows a significant change in compression-axis orientation from north to south within the study area. The *P* axes are near vertical in the north but range from near vertical to near horizontal in the south. A similar difference in *P*-axis orientation between northern and southern Utah is evident in Figure 9. Although the *P*-axis orientations from the study by Jones *et al.* (1985) show some scatter, they do appear to cluster around vertical. The *P*-axis orientations from the study by Arabasz and Julander (1986) range from near vertical to horizontal. Thus, the data from these two studies corroborate our observation of systematic changes in *P*-axis orientation within the study area.

Figures 7, 8, and 9 imply a change in the focal mechanisms of small earthquakes from north to south within central Utah. More specifically, small earthquakes along the Wasatch front north of about 40° represent predominantly normal faulting whereas those along the Wasatch front and Basin and Range/Colorado Plateau transition zone south of about 40°N display a mixture of normal, oblique-normal, and strike-slip faulting. Throughout the study area, the focal mechanisms that have a strike-slip component show a sense of slip consistent with the inferred E-W to ESE-WNW extension direction (Fig. 7). They indicate a component of left-lateral slip on N- to NE-striking nodal planes and a component of right-lateral slip on N- to NW-striking nodal planes, regardless of the direction of dip on these planes.

There is some geologic evidence that the change in contemporary faulting patterns from north to south in Utah indicated by the small earthquake focal mechanisms may also apply to larger earthquakes. Zoback (1983) summarizes slickenside data measured on primary faults in the Wasatch front region between 39°45′N and 42°10′N. Eight of the nine measurements are on NW- to NE-striking fault planes. These eight measurements show almost pure normal slip with rake angles ranging from 79° to 100°. The strike-slip component for six of these eight measurements matches the pattern identified in the focal mechanisms. The ninth set of measure-

ments, for the N80°E-striking Virginia Street fault at the northern end of Salt Lake City, shows right-lateral oblique-normal slip with rakes on two different slickenside sets of 143° and 172°. The faulting at this locality probably represents secondary faulting caused by a left step in the trace of the Wasatch fault (Fig. 1) (Pavlis and Smith, 1980; Zoback, 1983). In contrast to these fault slip measurements for northern Utah, Anderson and Barnhard (1987) have found abundant evidence for both strike-slip and normal faulting of late Cenozoic age in south-central Utah near Richfield. Their study was initiated after Arabasz and Julander (1986; see also Julander, 1983) found numerous strike-slip and oblique-slip focal mechanisms for small earthquakes in this region (Fig. 9).

The focal mechanism data summarized above have implications for the state of stress along the Wasatch front. Various authors have concluded that P and T axes of focal mechanisms, when they show preferred directions for a group of earthquakes, are reliable indicators of regional principal stress/strain directions (Zoback and Zoback, 1980; Kasahara, 1981; Sbar, 1982; Pechmann, 1987). This conclusion is based on mechanical arguments and on comparisons of these preferred directions with principal stress/strain directions determined from *in situ* stress measurements, geological data, and geodetic measurements. Zoback (1983) and Gephart and Forsyth (1984) found good agreement between principal stress directions determined from inversion of focal mechanism data and the average P- and T-axis directions. Most studies have used only the P and T axis of the best-fitting mechanism for each earthquake to calculate the mean compression and extension directions. The method used in this study also takes into account the degree of constraint of each focal mechanism, and should therefore give an improved estimate of these parameters.

The P and T axes for the study area north of 40°N (Figs. 8 and 9) suggest a stress field with principal axes oriented as follows: axis of minimum compressive principal stress, σ_3, horizontal and trending 96° ± 12°; axis of intermediate principal stress, σ_2, horizontal and trending 6° ± 12°; axis of maximum compressive principal stress, σ_1, vertical. If, following Zoback and Zoback (1980), we represent the magnitudes of principal stresses oriented east-west, north-south, and vertical by $\sigma_{E\text{-}W}$, $\sigma_{N\text{-}S}$, and σ_V, respectively, the inferred stress field can be specified by $\sigma_{E\text{-}W} < \sigma_{N\text{-}S} < \sigma_V$. The P and T axes for the area south of 40°N suggest a somewhat different stress field. Harmsen and Rogers (1986) demonstrated that, assuming a Coulomb-Navier criterion of slip, an axially symmetric extensional stress field with a horizontal least-principal stress $\sigma_3 < \sigma_2 = \sigma_1$ can accommodate both strike-slip and normal focal mechanisms as well as intermediate mechanisms with oblique slip. This kind of pattern is observed in the focal mechanisms of this study from the southern part of our study areas, and has been observed before in central and southern Utah by Arabasz and Julander (1986). Oblique-slip faulting may also result when preexisting faults slip in response to a reoriented triaxial stress field (Bott, 1959). Slemmons (1967), Zoback and Zoback (1980), and others have proposed that much of the oblique-slip normal faulting in the Basin and Range Province is due to preexisting faults that are not perpendicular to the uniform extension direction throughout much of the province. However, preexisting faults have a wide range of orientations in our study area. Mapped fault strikes generally range from NW to NE, but there are also some preexisting faults striking E-W in the study area (Hintze, 1980; Smith and Bruhn, 1984). We therefore conclude that the southern region focal mechanisms can best be explained by a stress field that has a horizontal least-principle stress axis trending about 96° ± 12° and intermediate- and maximum-principal stresses that are approximately equal in magnitude, i.e., $\sigma_{E\text{-}W} < \sigma_{N\text{-}S} \approx \sigma_V$. The range in P-

axis orientations from near vertical to near horizontal (Figs. 8 and 9) would therefore be a consequence of the similar magnitude of the maximum and intermediate principal stresses. This interpretation implies an increase in the magnitude of the intermediate principal stress, $\sigma_2 = \sigma_{N\text{-}S}$, relative to the magnitudes of the other principal stresses, from north to south along the Wasatch front.

The magnitude of σ_2 relative to σ_1 and σ_3 can be specified by the parameter ϕ (Bott, 1959):

$$\phi = \frac{\sigma_2 - \sigma_3}{\sigma_1 - \sigma_3}. \tag{3}$$

Since by definition, $\sigma_1 \geqq \sigma_2 \geqq \sigma_3$, it follows from (3) that $0 \leqq \phi \leqq 1$. The direction of the resolved shear stress across any new or preexisting fault plane is uniquely determined by ϕ and by the orientations of the principal stress axes. If it is assumed that (1) the orientations of the principle stress axes are known, and (2) the direction of slip on a fault coincides with the direction of the resolved shear stress, then it is possible to calculate ϕ from the strike and dip of the fault and the observed direction of slip.

The change in stress field that we infer from north to south along the Wasatch front implies an increase in ϕ from an intermediate value in the north to a high value (near one) in the south. As a test of this hypothesized stress change, we calculated ϕ values from our focal mechanisms using the principal stress axis orientations inferred above from the P and T axes. Various authors have developed techniques to simultaneously invert for both ϕ and the principal stress orientations from fault slip data obtained from slickensides or focal mechanisms (e.g., Angelier, 1979; Angelier *et al.*, 1982; Gephart and Forsyth, 1984; Michael, 1987). However, we did not attempt to apply these techniques to our data set because of the limited number of high-quality focal mechanisms.

Following Gephart (1985), we derived the following expression to calculate ϕ from a single observation of fault slip:

$$\phi = \frac{-(\hat{\mathbf{n}} \cdot \hat{\boldsymbol{\sigma}}_1)(\hat{\mathbf{b}} \cdot \hat{\boldsymbol{\sigma}}_1)}{(\hat{\mathbf{n}} \cdot \hat{\boldsymbol{\sigma}}_2)(\hat{\mathbf{b}} \cdot \hat{\boldsymbol{\sigma}}_2)}, \tag{4}$$

where $\hat{\mathbf{n}}$ is a unit vector perpendicular to the fault plane, $\hat{\mathbf{b}}$ is a unit vector perpendicular to $\hat{\mathbf{n}}$ and to the slip vector, and $\hat{\boldsymbol{\sigma}}_1$ and $\hat{\boldsymbol{\sigma}}_2$ are unit vectors in the directions of the maximum- and intermediate-principal stress axes, respectively. For our calculations, we assumed that $\hat{\boldsymbol{\sigma}}_1$ was vertical and that $\hat{\boldsymbol{\sigma}}_2$ was horizontal and had an azimuth of 6° ± 12°. We calculated ϕ values for each of the two nodal planes of our focal mechanisms, since we did not know which of the two represented the true fault plane. For each focal mechanism, only one of the two possible ϕ values that we calculated lies within the required range $0 \leqq \phi \leqq 1$. This result was expected because, as pointed out by Gephart (1985), for most focal mechanisms only one of the two possible fault planes is compatible with the assumption that the slip vector is parallel to the resolved shear stress on the plane. Note that the derivation of equation (4) does not take into account the sense of slip on the fault, e.g., normal or reverse, so the calculated ϕ values are only meaningful if the sense of slip is in the direction expected for the postulated stress field. In our data set, the slip directions indicated by the focal mechanisms for events SWW, ORE, and

WAP disagree with our assumed principal stress orientations, so we did not calculate ϕ values for these three mechanisms.

Tests showed that ϕ values calculated from equation (4) can be very sensitive to changes in nodal plane orientations. For this reason, we only report ϕ values for the A quality focal mechanisms (Table 3). The six ϕ values calculated from the A quality focal mechanisms range from 0.15 to 0.95 and have a mean value of 0.67 with a standard deviation of 0.36 (Table 3). Interestingly, the mean of the 14 ϕ values calculated from both the A and B quality focal mechanisms is the same, with a standard deviation of 0.31. These average ϕ values change by no more than 0.11 when the trend of $\hat{\sigma}_2$ is varied within the range of uncertainty of $\pm 12°$. Two of the ϕ values in Table 3 are <0.3 and the other four are >0.8. Both of the low ϕ values are from focal mechanisms in the northern Wasatch front region, but the other two ϕ values for this region are as high as the two values determined from focal mechanisms in the southern Wasatch front region. If both the A and B quality focal mechanisms are considered, the mean ϕ value for the northern Wasatch front region, 0.63 ± 0.32, is lower than the mean ϕ value for the southern Wasatch front region, 0.76 ± 0.30. However, the difference is less than half of the S.D.'s for these two means. Thus, although the calculated ϕ values provide some support for our hypothesized difference in average ϕ value between the northern and southern Wasatch front regions, the results are not conclusive because of the large scatter in the calculated ϕ values.

The stress field that we infer for the northern Wasatch front is in reasonable agreement with geodetic measurements of strain accumulation in this region. Triangulation surveys for the period 1962 to 1974 (Snay *et al.*, 1984) and trilateration surveys during the period 1972 to 1984 (Savage *et al.*, 1985) suggest a possible E-W to NW-SE extension across the Wasatch fault near Salt Lake City. However, the strain accumulation measured by these surveys is not significant at the 95 per cent confidence level.

Measurements of *in situ* stress in the Wasatch front region using the hydrofracturing technique indicate a stress field conducive to normal faulting, although results from different boreholes show variability in horizontal principal stress directions and relative magnitudes. Haimson (1984) and Haimson and Lee (1985) report on results from hydrofracturing stress measurements at 2 localities in northern Utah, 30-km SE of Salt Lake City and 25-km SE of Provo (Fig. 1). These measurements indicate a triaxial normal faulting stress regime with the direction of least-compressive principal stress in a NNE to NE general direction ($\sigma_{\text{NNE-SSW}} < \sigma_{\text{ESE-WNW}} < \sigma_V$). Zoback *et al.* (1981) used hydraulic fracturing to measure *in-situ* stress in a well located 25 km SE of Provo and only 500 m away from the second well of Haimson and Lee (1985) and Haimson (1984). Zoback *et al.* (1981) concluded that the average direction of the minimum horizontal principal stress was $73° \pm 15°$ and that the minimum horizontal principal stress was much less than both the

TABLE 3

ϕ VALUES FOR QUALITY FOCAL MECHANISMS

Region	Event Code	Strike	Dip	Rake	ϕ
Northern Wasatch front	HV3	153	41	−128	0.93
	BEL	156	46	−100	0.27
	OG3	230	43	−46	0.85
	SL1	174	33	−92	0.15
Southern Wasatch front	GOS	227	56	−39	0.88
	COF	224	59	−36	0.95

maximum horizontal principal stress and the vertical principal stress. However, further analysis has led them to revise their estimate of the azimuth of the minimum horizontal principal stress to 16 ± 15° (Zoback, 1989).

Zoback (1984) has discussed *in situ* stress data for the Wasatch front, most of which was from wells in the vicinity of the southern Wasatch fault zone between 39°N and 40°N. The data consist of wellbore elongations (breakouts) and hydraulic fractures, including the hydrofracture results from the two wells SE of Provo mentioned above. Taken together, these data suggest that the maximum principal stress is vertical but fail to show a strongly preferred orientation of the minimum horizontal stress in the region sampled. Therefore Zoback (1984) proposed that the Wasatch front region, north of approximately 39°N, is a normal faulting stress regime where the magnitudes of the two horizontal principal stresses, σ_2 and σ_3, are approximately equal (i.e., $\phi \approx 0$). In a stress regime of this kind, where $\sigma_{\text{E-W}} \approx \sigma_{\text{N-S}} < \sigma_{\text{V}}$, faulting should be predominantly normal dip-slip regardless of fault strike.

The southern region focal mechanisms of this study (Fig. 7) have locations similar to the *in situ* stress data of Zoback (1984). These mechanisms have significant strike-slip components, especially when the 'fair' solutions are also taken into account. Furthermore, the ϕ values calculated from our two A quality focal mechanisms in this region are both high, near 0.9 (Table 3). Arabasz and Julander (1986) have also determined a number of focal mechanisms of earthquakes with locations between latitudes 39° and 40°N. Many of their mechanisms also indicate strike-slip and oblique-normal-slip faulting (Fig. 9). Therefore, available focal mechanism data in the vicinity of the southern Wasatch fault zone in central Utah do not support Zoback's hypothesis of a normal faulting stress regime with $\phi = 0$.

Conclusions

Focal mechanisms determined in this study and in other studies indicate that small earthquakes in the Wasatch front region of Utah are accommodating E-W to ESE-WNW extension in the upper crust by slip on faults of moderate to steep dip (>30°). The available data show predominantly normal faulting north of 40°N and a mixture of normal, oblique-normal, and strike-slip faulting south of 40°N. This observation suggests a possible change in stress state from a normal faulting regime in the northern Wasatch front region with

$$\sigma_{\text{E-W}} < \sigma_{\text{N-S}} < \sigma_{\text{V}}$$

to a normal and strike-slip faulting regime in the southern Wasatch front region with

$$\sigma_{\text{E-W}} < \sigma_{\text{N-S}} \approx \sigma_{\text{V}}$$

Focal mechanisms in both regions are consistent on a regional scale with late Cenozoic faulting patterns inferred from geologic evidence. The normal faulting mechanisms found in northern Utah reflect the ongoing extension of the eastern-most Basin and Range Province. The normal, oblique-normal, and strike-slip focal mechanisms in central Utah may be the result of a transitional stress field between the extensional tectonics of the Basin and Range Province and the compressional tectonics of the northwestern Colorado Plateau.

ACKNOWLEDGMENTS

We thank John M. Bartley, Robert B. Smith, Ivan G. Wong, and especially Walter J. Arabasz for useful discussions regarding this work. Ivan Wong also supplied copies of film records from the Woodward-Clyde Consultants network in southeastern Utah. Craig H. Jones generously allowed us to include in Figure 9 his recently completed focal mechanisms of microearthquakes in Hansel and Pocatello Valleys. Erwin McPherson and Ken Whipp provided records on the maintenance of seismograph stations that were very helpful in identifying polarity reversals, and tested some station polarities in the field using a tool that they developed for this purpose. This paper benefited from reviews by Mary Lou Zoback, Walter J. Arabasz, and Ethan D. Brown. Charles M. Schlinger and Gerald W. Hohmann reviewed the M.S. thesis on which this paper was based. This research was supported by the U.S. Geological Survey, Department of the Interior, under award numbers 14-08-0001-G1163 and 14-08-0001-G1349. Partial support also came from a scholarship awarded by the Society of Exploration Geophysicists and sponsored by the Sohio Petroleum Company.

REFERENCES

Aki, K. and P. G. Richards (1980). *Quantitative Seismology: Theory and Methods*, W. H. Freeman, San Francisco, California, 932 pp.

Anderson, R. E. and T. P. Barnhard (1987). Neotectonic framework of the central Sevier Valley area, Utah, and its relationship to seismicity, in *Assessment of Regional Earthquake Hazards and Risk Along the Wasatch Front, Utah*, P. L. Gori and W. W. Hays, Editors, *U.S. Geol. Surv., Open-File Rept. 87-585*, F1-F134 (also, *U.S. Geol. Surv. Profess. Paper*, in press).

Angelier, J. (1979). Determination of the mean principal directions of stress for a given fault population, *Tectonophysics* **56,** T17–T26.

Angelier, J. A., A. Tarantola, B. Valette, and S. Manoussis (1982). Inversion of field data in fault tectonics to obtain the regional stress, I, Single phase fault populations: a new method of computing the stress tensor, *Geophys. J. R. Astr. Soc.* **69,** 607–621.

Arabasz, W. J. and D. R. Julander (1986). Geometry of seismically active faults and crustal deformation within the Basin and Range-Colorado Plateau transition, in *Cenozoic Tectonics of the Basin and Range Province: A Perspective on Processes and Kinematics of an Extensional Origin*, L. Mayer, Editor, *Geol. Soc. Am. Special Paper* 208, 43–74.

Arabasz, W. J., J. C. Pechmann, and E. D. Brown (1987). Observational seismology and the evaluation of earthquake hazards and risk in the Wasatch front area, Utah, in *Assessment of Regional Earthquake Hazards and Risk Along the Wasatch Front, Utah*, P. L. Gori and W. W. Hays, Editors, *U.S. Geol. Surv., Open-File Rept. 87-585*, D1-D58 (Also *U.S. Geol. Surv. Profess. Paper*, in press).

Arabasz, W. J., W. D. Richins, and C. J. Langer (1981). The Pocatello Valley (Idaho-Utah border) earthquake sequence of March to April 1975, *Bull. Seism. Soc. Am.* **71,** 803–826.

Arabasz, W. J. and R. B. Smith (1981). Earthquake prediction in the Intermountain seismic belt—An intraplate extensional regime, in *Earthquake Prediction—An International Review*, Maurice Ewing Series, Vol. 4, D. W. Simpson and P. G. Richards, Editors, American Geophysical Union, Washington, D. C., 238–258.

Arabasz, W. J., R. B. Smith, and W. D. Richins, Editors (1979). *Earthquake Studies in Utah, 1850 to 1978*, Special Publication, University of Utah Seismograph Stations, Salt Lake City, 552 pp.

Arabasz, W. J., R. B. Smith, and W. D. Richins (1980). Earthquake studies along the Wasatch Front, Utah: network monitoring, seismicity, and seismic hazards, *Bull. Seism. Soc. Am.* **70,** 1479–1499.

Bjarnason, I. T. (1987). Contemporary tectonics of the Wasatch front region, Utah, from earthquake focal mechanisms, *M.S. Thesis*, University of Utah, Salt Lake City, Utah, 79 pp.

Bott, M. H. P. (1959). The mechanics of oblique slip faulting, *Geological Magazine* **96,** 109–117.

Braile, L. W., R. B. Smith, G. R. Keller, and R. M. Welch (1974). Crustal structure across the Wasatch Front from detailed seismic refraction studies, *J. Geophys. Res.* **79,** 2669–2677.

Brown, E. D., W. J. Arabasz, I. Bjarnason, and K. Quigley (1986). The March 1986 M_L 4.4 Japanese Valley, Utah, earthquake sequence: a type-case study for central Utah, *EOS* **67,** 1107.

Fenneman, N. M. (1946). Physical divisions of the United States, U.S. Geol. Surv. Map, scale 1:7,000,000.

Gephart, J. W. (1985). Principal stress directions and the ambiguity in fault plane identification from focal mechanisms, *Bull. Seism. Soc. Am.* **75,** 621–625.

Gephart, J. W. and D. W. Forsyth (1984). An improved method for determining the regional stress tensor using earthquake focal mechanism data: application to the San Fernando earthquake sequence, *J. Geophys. Res.* **89,** 9305–9320.

Gori, P. L. and W. W. Hays, Editors (1987). Assessment of Regional Earthquake Hazards and Risk

Along the Wasatch Front, Utah, *U.S. Geol. Surv., Open-File Rept. 87-585* (Also *U.S. Geol. Surv. Profess. Paper*, in press).

Haimson, B. C. (1984). Stress measurements in the Wasatch hinterland complement existing tectonic and seismic data, *EOS* **65,** 1118.

Haimson, B. C. and M. Y. Lee (1985). Stress measurements at the Jordanelle dam site, central Utah, using wireline hydrofracturing, *Final Rept. to U.S. Geol. Surv.*, 34 pp.

Harmsen, S. C. and A. M. Rogers (1986). Inferences about the local stress field from focal mechanisms: applications to earthquakes in the southern Great Basin of Nevada, *Bull. Seism. Soc. Am.* **76,** 1560–1572.

Hintze, L. F. (1980). Geologic map of Utah, Utah Geological and Mineral Survey Map, scale 1:500,000.

Johnson, P. A. and M. L. Sbar (1987). A microearthquake study of southwest Utah-northwest Arizona: transition between the Basin and Range Province and Intermountain seismic belt, *Bull. Seism. Soc. Am.* **77,** 579–596.

Jones, C. H. (1987). A geophysical and geological investigation of extensional structures, Great Basin, western United States, *Ph.D. Thesis*, Massachusetts Institute of Technology, Cambridge, Massachusetts, 226 pp.

Jones, C. H., P. H. Molnar, R. B. Smith, and G. Chen (1985). Microearthquake investigation of the Hansel Valley-Pocatello Valley region, northern Utah and southern Idaho, *EOS* **66,** 954.

Julander, D. R. (1983). Seismicity and correlation with fine structure in the Sevier Valley area of the Basin and Range-Colorado Plateau transition, south-central Utah, *M.S. Thesis*, University of Utah, Salt Lake City, Utah, 143 pp.

Kasahara, K. (1981). *Earthquake Mechanics*, Cambridge University Press, Cambridge, 248 pp.

Keller, G. R., R. B. Smith, and L. W. Braile (1975). Crustal structure along the Great Basin-Colorado Plateau transition from seismic refraction studies, *J. Geophys. Res.* **80,** 1093–1098.

Klein, F. W. (1978). Hypocenter location program HYPOINVERSE, *U.S. Geol. Surv., Open-File Rept. 78-694*, 102 pp.

Loeb, D. T. (1986). The *P*-wave velocity structure of the crust-mantle boundary beneath Utah, *M.S. Thesis*, University of Utah, Salt Lake City, Utah, 126 pp.

Loeb, D. T. and J. C. Pechmann (1986). The *P*-wave velocity structure of the crust-mantle boundary beneath Utah from network travel time measurements, *Earthquake Notes* **57** (1), 10.

Martin, W. R. (1978). A seismic refraction study of the northeastern Basin and Range and its transition with the eastern Snake River Plain, *M.S. Thesis*, University of Texas at El Paso, El Paso, Texas, 41 pp.

McKee, M. E. and W. J. Arabasz (1982). Microearthquake studies across the Basin and Range-Colorado Plateau transition in central Utah, in *Overthrust Belt of Utah*, D. L. Nielson, Editor, *Utah Geological Association, Publication 10*, 137–149.

Meissner, R. (1986). *The Continental Crust: A Geophysical Approach*, Academic Press, Orlando, Florida, 426 pp.

Michael, A. J. (1987). Use of focal mechanisms to determine stress: A control study, *J. Geophys. Res.* **92,** 357–368.

Mueller, S. (1977). A new model of the continental crust, in *The Earth's Crust*, J. Heacock, Editor, *American Geophysical Union Monograph* **20,** 289–317.

Muller, G. and S. Mueller (1979). Travel-time and amplitude interpretation of crustal phases on the refraction profile Delta-W, Utah, *Bull. Seism. Soc. Am.* **69,** 1121–1132.

Pavlis, T. L. and R. B. Smith (1980). Slip vectors on faults near Salt Lake City from Quaternary displacements and seismicity, *Bull. Seism. Soc. Am.* **70,** 1521–1526.

Pechmann, J. C. (1987). Tectonic implications of small earthquakes in the central Transverse Ranges, in Recent Reverse Faulting in the Transverse Ranges, California, *U.S. Geol. Surv. Profess. Paper 1339*, 97–111.

Pechmann, J. C., W. D. Richins, and R. B. Smith (1984). Evidence for a "double moho" beneath the Wasatch front, Utah, *EOS* **65,** 988.

Roller, R. C. (1965). Crustal structure in the eastern Colorado Plateau province from seismic refraction measurements, *Bull. Seism. Soc. Am.* **55,** 107–119.

Savage, J. C., M. Lisowski, and W. H. Prescott (1985). Strain accumulation in the Rocky Mountain states, *J. Geophys. Res.* **90,** 10,310–10,320.

Sbar, M. L. (1982). Delineation and interpretation of seismotectonic domains in western North America, *J. Geophys. Res.* **87,** 3919–3928.

Schwartz, D. P. and K. J. Coppersmith (1984). Fault behavior and characteristic earthquakes: examples from the Wasatch and San Andreas fault zones, *J. Geophys. Res.* **89,** 5681–5698.

Slemmons, D. B. (1967). Pliocene and Quaternary crustal movements of Basin and Range province,

USA, *Journal of Geoscience* **10,** 91–101.

Smith, R. B. (1978). Seismicity, crustal structure, and intraplate tectonics of the interior of the western Cordillera, in *Cenozoic Tectonics and Regional Geophysics of the Western Cordillera*, R. B. Smith and G. P. Eaton, Editors, *Geol. Soc. Am. Mem.* **152,** 111–144.

Smith, R. B. and R. L. Bruhn (1984). Intraplate extensional tectonics of the eastern Basin-Range: inferences on structural style from seismic reflection data, regional tectonics, and thermal-mechanical models of brittle-ductile deformation, *J. Geophys. Res.* **89,** 5733–5762.

Smith, R. B. and A. G. Lindh (1978). Fault-plane solutions of the western United States: a compilation, in *Cenozoic Tectonics and Regional Geophysics of the Western Cordillera*, R. B. Smith and G. P. Eaton, Editors, *Geol. Soc. Am. Mem.* **152,** 107–109.

Smith, R. B. and M. L. Sbar (1974). Contemporary tectonics and seismicity of the western United States with emphasis on the Intermountain seismic belt, *Geol. Soc. Am. Bull.* **85,** 1205–1218.

Snay, R. A., R. B. Smith, and T. Soler (1984). Horizontal strain across the Wasatch front near Salt Lake City, Utah, *J. Geophys. Res.* **89,** 1113–1122.

Sparlin, M. A., L. W. Braile, and R. B. Smith (1982). Crustal structure of the eastern Snake River Plain determined from ray trace modeling of seismic refraction data, *J. Geophys. Res.* **87,** 2619–2633.

Thompson, G. A. and M. L. Zoback (1979). Regional geophysics of the Colorado Plateau, *Tectonophysics* **61,** 149–181.

Vetter, U. and A. S. Ryall (1983). Systematic change of focal mechanism with depth in the western Great Basin, *J. Geophys. Res.* **88,** 8237–8250.

Whitcomb, J. H. (1973). The 1971 San Fernando earthquake series focal mechanisms and tectonics, *Ph.D. Thesis (Part II)*, California Institute of Technology, Pasadena, California.

Williams, D. J. and W. J. Arabasz (1985). Mining-related seismicity in the East Mountain area, Wasatch Plateau, centeral Utah, *EOS* **66,** 954.

Williams, D. J. and W. J. Arabasz (1989). Mining-related and tectonic seismicity in the East Mountain area, Wasatch Plateau, Utah, U.S.A., *Pure Appl. Geophys*, in press.

Wong, I. G. and J. R. Humphrey (1989). Contemporary seismicity, faulting and the state of stress in the Colorado Plateau (submitted for publication).

Wong, I. G., J. R. Humphrey, and R. W. Ely (1987). The contemporary state of stress in the Colorado Plateau, *Geol. Soc. Am. Abstracts with Programs* **19,** 896.

Zoback, M. L. (1983). Structure and Cenozoic tectonism along the Wasatch fault zone, Utah, in *Tectonics and Stratigraphy of the Great Basin*, D. M. Miller, V. R. Todd, and K. A. Howard, Editors, *Geol. Soc. Am. Mem.* **157,** 3–27.

Zoback, M. L. (1984). Constraints on the in-situ stress field along the Wasatch front, in *Proceedings of Conference XXVI, a Workshop on Evaluation of Regional and Urban Earthquake Hazards and Risk in Utah*, W. W. Hays and P. L. Gori, Editors, *U.S. Geol. Surv., Open-File Rept. 84-763*, 286–309.

Zoback, M. L. (1989). State of stress and modern deformation of the northern Basin and Range province, *J. Geophys. Res.* (in press).

Zoback, M. L. and M. D. Zoback (1980). State of stress in the conterminous United States, *J. Geophys. Res.* **85,** 6113–6156.

Zoback, M. D., M. L. Zoback, J. Svitek, and R. Liechti (1981). Hydraulic-fracturing stress measurements near the Wasatch fault, central Utah, *EOS* **62,** 394.

DEPARTMENT OF GEOLOGY AND GEOPHYSICS
UNIVERSITY OF UTAH
SALT LAKE CITY, UTAH 84112-1183

Manuscript received 8 August 1987